Magnetic field effects of photocarrier generation in bulk heterojunctions at low temperature

Magnetic field effects of photocarrier generation in bulk heterojunctions at low temperature

H. Tajima,[*a,b] Y. Nishioka,[a] S. Sato,[a] T. Suzuki,[b] M. Kimata[b]

[a]*Graduate School of Material Science, University of Hyogo,*
3-2-1 Kohto, Kamigori-cho, Ako-gun, Hyogo 678-1297, Japan.
E-mail: tajima@sci.u-hyogo.ac.jp

[b]*Institute for Solid State Physics, The University of Tokyo,*
Kashiwa, Chiba 277-8581, Japan

ABSTRACT

We report an experimental investigation of the magnetic field effect (MFE) in polymer bulk heterojunction devices at temperatures below 10 K using photocarrier extraction by linearly increasing voltages. The examined devices were composed of an active layer of poly(3-hexylthiophene) and [6,6]-phenyl-C_{61}-butyric acid methyl ester. In the experiments, the delay time (t_d) dependence of the MFE was investigated in detail. For $t_d < 80$ μs, a positive MFE was observed in the field region $B < 0.1$ T and a negative MFE was observed for $B > 0.2$ T. For $t_d > 8$ ms, only a positive MFE proportional to B^2 was observed. For the photocurrent pulse detected immediately after light irradiation, the MFE was negligibly small. In a high magnetic field of 15 T, a significant MFE exceeding 80% was observed at 1.8 K for $t_d = 800$ ms. We discuss the results based on a model of triplet-singlet (or singlet-triplet) conversion in the magnetic field and estimate the exchange integral for the charge-transfer exciton in this photovoltaic cell.

Introduction

Magnetic field effects (MFEs) in thin-film organic devices have recently been intensively studied in terms of electroluminescence (EL), charge current, and photocurrent; the relevant field is known as "organic spintronics".

This field includes two main categories of research. The first category involves the study of phenomena related to spin current,[1-5] which are similar to those examined by inorganic spintronics. The second category investigates MFEs, which are noticeable even in extremely low field ranges.[6-15] In these studies, spin current is not the target. Organic magnetoresistance (OMAR) is a typical phenomenon examined in this category.[8] The present study is classified in this group.

To date, several models have been suggested to explain OMAR and its related phenomena in the steady states: the electron-hole pair model,[9, 7] the exciton-exciton interaction model,[16] the exciton-charge interaction model,[11] and the bipolaron model.[10] Although the detailed mechanism of MFEs considered in these models is different, their common assumption is that MFEs are associated with a dynamic process of extinction and generation of charge carriers and excitons. In other words, MFEs in organic thin-film devices are not a phenomenon occurring in a thermal equilibrium state. This indicates that time dependence experiments are crucial for clarifying the mechanism of MFEs. However, few experimental studies that examine the time dependence of MFEs have been reported.[17, 18] In this paper, we report on the time dependence of MFEs observed in photocarrier extraction experiments using a linearly increasing voltage (photo-CELIV). The photo-CELIV technique was originally developed to determine the time and field dependence of the hopping conduction mobility of charge carriers generated by a light pulse.[19, 20] In this technique, a strongly bound Frenkel exciton is initially formed by the light pulse under zero- or finite-bias voltages. The Frenkel exciton (FRE) changes into a weakly bound charge-transfer exciton (CTE) within a very short time of the order of a few tens of femtoseconds. Because the binding energy of the CTE is not very large, the CTE can dissociate into charge carriers in an applied electric field or by thermal energy. In the present photo-CELIV experiments, the extraction current associated with the charge carriers that were formed by this dissociation was measured using a linearly increasing ramping voltage that was applied after an arbitrarily chosen delay time t_d.

Time-resolved experiments based on the photo-CELIV technique have two main advantages: First, we can directly determine the density function of the CTE from the observed photo-CELIV signal at low temperature. Second, in photo-CELIV

experiments, the lifetime of the photogenerated CTE can be investigated under the zero-bias-voltage condition, in contrast to time-of-flight experiments, in which a constant bias voltage is applied throughout the measurement.[21]

Experiments

Figure 1 shows the structures of the devices used in the measurements. Sample (a) was a conventional polymer bulk-heterojunction photovoltaic cell.[22] The indium-tin oxide (ITO) and Al electrodes operated as a cathode and an anode, respectively. The thicknesses of the poly(3-hexylthiophene): [6,6]-phenyl-C61-butyric acid methyl ester (P3HT:PCBM) active layer, the poly(3,4-ethylenedioxythiophene): poly(styrenesulfonate) (PEDOT:PSS) hole-transport layer, and the Al electrode were 130, 30, and 60 nm, respectively. Details on the fabrication method have been reported elsewhere.[23] This sample was used in measurements performed in a high magnetic field up to 15 T. Sample (b) was an inverted-type polymer photovoltaic cell. In this cell, the dipole in the thin layer of polyethyleneimine (PEI) effectively reduced the work function of the ITO from 4.6 eV to 3.5 eV.[24] Consequently, the ITO electrode functioned as an anode in this cell. The inverted-type photovoltaic cell had an advantage regarding its stability in the atmosphere, because a stable metal electrode covered the top of the sample device. The thicknesses of the PEI, P3HT:PCBM active layer, MoO_3 hole-transport layer, and Ag electrode in this cell were 10, 100, 15, and 45 nm, respectively. This sample was used in measurements performed in low and intermediate magnetic fields.

Figure 1c shows the experimental scheme for the photo-CELIV measurements. $J(t)$ and $V(t)$ on the vertical axis correspond to the extracted current density and reverse-bias voltage, respectively, and t on the horizontal axis denotes the time. In these measurements, photocarriers were generated inside the photovoltaic cell using a light pulse. After a delay time of t_d, the carriers were extracted using a linearly ramping reverse-bias voltage with rate A. Considering that the sample device behaved as a capacitor for an applied reverse-bias voltage, a step-like displacement current was expected for ramping under dark conditions. A very small deviation of the dark extraction current from the step-like form is due to charge carrier injection under thermal conditions.[25] When the sample was irradiated before ramping, the CELIV signal appeared; this corresponded to the additional current due to the photo-generated carriers.[19, 20] In this measurement, we used a triangle-shaped voltage waveform instead of a sawtooth-shaped one, which is used in conventional CELIV measurements. The advantage of the triangular waveform is that the CELIV signal can be measured both in

the ascending and descending sweeps. The offset voltage V_0 was zero except in the pulse signal measurements. To ensure the accuracy of the signal integration, the pulse signal was measured separately under an applied offset voltage of 2.5 V or 3 V.

The measurements were performed below 10 K where MFEs are enhanced. In the high-field (up to 15 T) experiments, we used a solenoid magnet (OXFORD Inst.) and a neodymium-doped yttrium aluminum garnet (Nd:YAG) laser-pumped optical parametric oscillator (OPO) as the light source for the photo-CELIV measurements. The excitation wavelength was selected to be 520 nm and the light intensity was 4.5±0.2 mJ mm^{-2} pulse^{-1}. In the low- and intermediate-field experiments, we used a split-pair magnet (Cryogenic Limited), and the second harmonics of the YAG laser (532 nm). The light intensity (approximately 2.7 μJ) was monitored throughout the measurement to correct the signal intensity. Based on this correction, we could suppress the error associated with the light-intensity fluctuation to below 0.2%. The pulse widths of the OPO and YAG were lower than 10 ns.

Results

(a) Photo-CELIV measurement in a high magnetic field

Figures 2a–d show comparisons of the CELIV signals obtained in the magnetic fields of $B = 0$ T and 15 T as a function of the electric field. The temperature was $T = 1.8$ K or 5 K, the delay time $t_d = 8$ μs or $t_d = 800$ ms, and the speed of the voltage increase was $A = 20000$ V/s. In the magnetic field, the CELIV signals increased in amplitude and the peaks of the signals shifted to the right. In order to examine the shift closely, we plotted the magnification of the data at 0 T as shown by the green solid lines. As can be seen from the plot, the shift at $F = 2.5 \times 10^7$ V/m is 0.2–0.3 × 10^7 V/m for $t_d = 800$ ms (Figs. 2b and 2d) and ~0.1 × 10^7 V/m for $t_d = 8$ μs (Figs. 2a and 2c). The increase of the CELIV amplitude became more obvious as the temperature decreased and the delay time increased.

We evaluated the *MFE(B)*, which is defined as

$$MFE(B) = (I(B) - I(0)) / I(0), \tag{1}$$

where $I(B)$ is the integrated intensity of the CELIV signal in field B. The obtained values of *MFE*(15 T) at $T = 5$ K were 0.6±4% for $t_d = 8$ μs and 18±4% for $t_d = 800$ ms. The corresponding values at 1.8 K were 24±4% for $t_d = 8$ μs and 85±4% for $t_d = 800$ ms.

The CELIV signal J_{CE} at low temperatures below 100 K is well described by the Poole-Frenkel model.[26] The CTE density ρ as a function of dissociation energy ε is

provided by J_{CE} at $T = 0$ K under the assumption of infinite mobility for the charge carriers using the following relation:[23]

$$\frac{J_{CE}(F)}{A} = \frac{e\beta F^{-1/2}}{2} \rho\left(\beta F^{1/2}\right),$$ (2)

where F is the electric field, β is the Poole-Frenkel parameter, and e is the elementary charge. This equation is useful for the quantitative analysis of the photo-CELIV data at extremely low temperatures. However, the application of this equation involves two requirements: First, the deformation of the CELIV signal due to the finite mobility effect must be avoided; this effect is considerable for large voltage ramping speeds. Secondly, the deformation of the CELIV signal due the self-quenching of the CTE must be avoided. Because self-quenching is dominant immediately after the light irradiation, a larger value of t_d is favorable for avoiding this effect. Then we chose the parameters of $A = 2000$ V/s and $t_d = 8$ ms, and evaluated the density function at 0 T and 15 T. Figures 1e and 1f show the CELIV measured signal at $T = 1.8$ K, and the density function derived from the observed signal using Eq. (2) with $\beta = 1.2 \times 10^{-5}$ eV m$^{0.5}$ V$^{-0.5}$, respectively.[27] The obtained density functions are well expressed by the Gaussian function

$$\rho(\varepsilon) = D\exp\left\{-(\varepsilon - \varepsilon_0)^2 / \sigma^2\right\}$$ (3)

with the parameters listed in Table 1. A drastic increase of D, and a small increase of ε_0 are obvious. As we discuss later in detail, the changes of the parameters are due to the singlet-triplet (S-T) conversion of the CTE. The peak shift reflects the dissociation-energy difference between the singlet and triplet CTEs. If we evaluate the peak shift directly from the Gaussian parameters, the shift is 0.007 eV. However, considering that only half of the Gaussian profile is available in the fitting procedures, the above shift value is not convincing. Thus, we evaluated the shift directly from the plots of 15 T and 0 T (×1.7; green solid line) data, to obtain a shift value of ~0.003 eV. Although this is a simple technique, we think the obtained value is more reliable.

(b) Photo-CELIV measurement in low ($B < 0.2$ T) and intermediate ($B < 3$ T) magnetic field

The high-field experiments revealed that the CELIV signal drastically increased in the magnetic field and the delay time influenced the field dependence. However, the detailed field and delay time dependence was not investigated. Subsequently, we examined $MFE(B)$ for various values of t_d. As shown in Fig. 3, which displays the $MFE(B)$ for $B < 0.2$ T, the field dependence of the pulse signal immediately after the light irradiation was rather small. On the other hand, the CELIV signals at $t_d = 8$ μs and 800 μs exhibit a positive and cusp-like field dependence of $MFE(B)$. For $t_d > 800$ μs, $MFE(B)$ decreases and for $t_d > 8$ ms, it is negligible.

Figure 4 shows $MFE(B)$ at several t_d values in the field range $B < 3$ T. The black solid line shows $MFE(B)$ at $t_d = 8$ μs as a guide for the eyes. In the intermediate field range ($B > 0.2$ T), $MFE(B)$ is negative for $t_d \leq 80$ μs and changes to be positive for $t_d \geq 400$ μs. For the pulse signal, $MFE(B)$ is also relatively small in this region.

When t_d is larger than 8 ms, $MFE(B)$ is approximately proportional to B^2. The red solid line shows the least-squares fit of cB^2 to the data measured at $t_d = 800$ ms. Parameter c was 0.53×10^{-2} T^{-2}.

Figure 5 shows the delay time dependence of the CELIV signal intensity for the fields $B = 0, 0.1, 3$ T; note the logarithmic scale of the horizontal axis. The CELIV signal intensity exhibits a non-exponential time dependence, i. e., a rapid decrease for small t_d and a very slow decay for large t_d. Because the CELIV signal intensity reflects the CTE population, the figure demonstrates that CTE has very long life time at 2.0 K. The inversion of the MFE occurs at approximately $t_d = 300$ μs. For $t_d > 300$ μs, the decrease of the CELIV signal is larger at zero field than in the magnetic field. For $t_d < 300$ μs, the CELIV signal intensity at zero field is between the intensities observed at $B = 0.1$ T and $B = 3$ T. This is consistent with the data shown in Fig. 3.

Discussion

Figure 6 shows the energy level diagram summarizing the main processes involved in charge photogeneration in the bulk-heterojunction photovoltaic cell.[28-30] In the photovoltaic cell, the singlet FRE, a strongly bound electron-hole pair, is formed in either the donor or the acceptor molecule immediately after the light irradiation. The FRE migrates to the donor-acceptor boundary and is converted into a CTE within several tens of femtoseconds. The CTE dissociates in the weak electric field or by thermal energy to form free positive and negative polarons (P^+ or P^-), which carry the charge current. Some of the free polarons recombine through bimolecular recombination to occupy a polaron pair (PP) state. In photo-CELIV experiments, we can control the charge generation process (k_{3ST}, k_{6ST}) through the applied electric field.

In the following discussion, we apply the electron-hole pair model to the diagram of Fig. 6 and examine the origin of the MFEs observed in this study. In this model, we assume a nearly zero exchange interaction for the electron-hole pair. In this situation, an electron-hole pair undergoes an S-T (or T-S) conversion. This conversion is influenced by the magnetic field and causes the MFEs, because of the different rate constants associated with the singlet and triplet pairs. For example, consider the case of an excited triplet species with a lifetime longer than that of singlet species being the precursor. Singlet species are formed from the triplet species through the T-S conversion. Consequently, the T-S conversion results in the decrease of the number of the excited species, of the carrier density, and of the photocurrent. The reverse occurs in the case of a singlet precursor.

Under the condition of nearly zero exchange interaction, several mechanisms of the S-T (or T-S) conversion are known.[14, 31] The hyperfine-coupling mechanism takes into account the off-diagonal matrix elements between the singlet and the three triplet sub-levels derived from the hyperfine coupling interaction. The three triplet sub-levels and the singlet level are degenerate at zero field but two of the triplet sub-levels separate in a finite magnetic field owing to the Zeeman effect. Consequently, the rate of the S-T (or T-S) conversion is highest at zero field and decreases in the finite magnetic field. The Δg effect arises from the difference of the electron and hole g factors. The S-T (or T-S) conversion due to this mechanism has a zero rate at zero field and increases with increasing magnetic field. When we consider the two mechanisms affecting the excited triplet precursor, a positive MFE is expected for the photocurrent near zero field owing to the hyperfine-coupling mechanism and a negative MFE for the photocurrent in the high-field region because of the Δg mechanism. The reverse occurs for the excited singlet precursor.

Another important mechanism to cause the S-T conversion is thermal spin polarization.[32,33] In this mechanism, thermal relaxation towards a stable spin state in a magnetic field is considered. This relaxation occurs in a similar time-scale to that of the spin-relaxation time. Unlike the Δg and hyperfine-coupling mechanisms, S-T conversion due to this mechanism occurs even though the exchange constant J is large. The singlet species are required to have a life time longer than the spin-relaxation time. Because the Zeeman energy is more than the thermal energy under a magnetic field of 15 T below 5 K, this mechanism should be especially important for the MFE data at 15 T.

The above scenario for the MFE concerns the singlet and triplet species of one excited state. In organic thin-film devices, we must consider the S-T (or T-S) conversion

for three excited states (FRE, CTE, and PP), as shown in Fig. 6; consequently, the situation is more complicated. In the following, we discuss the origin of the MFEs of the photo-CELIV signal based on this framework.

First, we discuss the relatively small MFE observed for the pulse signal immediately after the light irradiation, as shown in Fig. 3 and Fig. 4. The pulse signal arises from the direct dissociation of the singlet FRE or the dissociation of the CTE produced by the singlet FRE. In either case, an MFE is expected in the pulse signal if an S-T conversion occurs in the FRE. Therefore, the absence of MFEs indicates that the FRE is not associated with the MFE. Because the FRE exhibits strong exchange coupling, no S-T conversion or resulting MFEs should be expected for FRE.[12] This concept is consistent with our observations.

Secondly, we discuss the CELIV signal for a delay time $t_d < 80$ μs. As shown in Figs. 3 and 4, in this delay time range, a positive $MFE(B)$ is observed for a field of $B < 0.1$ T and a negative one for $B > 0.2$ T. This MFE is explained by considering the hyperfine and Δg effects for the triplet precursor. Because no S-T conversion is expected for singlet FREs with large exchange interaction, singlet species are expected to be dominant for the CTE immediately after its formation. On the other hand, the dominant species of the PP, which is formed as a result of bimolecular recombination of free polarons, should be the triplet. Thus, it is plausible that in this delay time region, MFE is governed by the triplet precursor of the PP. The quench of MFE in the weak field region for $t_d > 8$ ms is possibly due to the saturation of the T-S conversion. According to Devir-Wolfman et al.,[34] a positive MFE for the photocurrent of a P3HT:PCBM bulk heterojunction in the weak-field range is assigned to the PP. This conclusion is consistent with our analysis, as described above.

The behavior in the intermediate region 80 μs$<t_d< 8$ ms seems to be described by the combined effects governing the MFEs in the regions $t_d < 80$ μs and $t_d > 8$ ms. Thus we omit the relevant discussion here. Next, we discuss the CELIV signal for $t_d > 8$ ms. In this delay time region, no MFE was observed in the weak-field region $B < 0.1$ T and a positive MFE, approximately proportional to B^2, was measured in the high-field region. This behavior is consistent with the gigantic MFE shown in Fig. 2 and is attributable to the S-T conversion in a magnetic field. As discussed above, the singlet species is expected to be dominant for the CTE immediately after its formation. Therefore, the MFE in this delay time region is attributable to S-T conversion owing to the singlet precursor of the CTE. This consideration is again consistent with the conclusion of Devir-Wolfman et al.[34] Here, we should emphasize the absence of weak-field MFE and the B^2 dependence of the high-field MFE; this behavior is different

from that of the PP triplet precursor for $t_d \leq 80$ µs. The most plausible explanation for this behavior is non-negligible exchange interaction J for the CTE.

In this context, the shift of the peak for the CTE density function shown in Fig. 2f is noteworthy. The CTE, immediately after formation, should be in the singlet state, and the magnetic field should enhance the S-T conversion either by Δg mechanism or by thermal polarization. Consequently, the triplet ratio of the CTE should be higher at 15 T than in the zero field. Then, a peak shift of $\Delta \varepsilon_0 = 0.003$ eV provides the lowest estimate for the dissociate energy difference between the singlet and triplet species of the CTE. The dissociation energy does not contain any contribution from the Zeeman effect because the dissociation of the electron-hole pair due to electric field does not cause rotation of spins. Then, we simply evaluated the exchange interaction $2J > 0.003$ eV. As the exchange interaction reduces the energy of the triplet CTE, the dissociation energy of the triplet CTE, which is dense in the magnetic field, should be larger than that of the singlet CTE. Thus a peak shift towards the high-energy side under the magnetic field is expected. This consideration is consistent with the observation.

Because the magnetic field $B_J = J/g\mu_B > 13$ T is very large, the rate constant, which causes S-T conversion of the CTE due to the Δg effect, should be very small. In such a case, the total rate constant of the S-T conversion (sum of the rate constants due to the Δg effect and thermal polarization effect) should also be small. This is consistent with the observations that the MFE associated with the CTE explicitly appears for $t_d > 8$ ms, while the MFE associated with PP is evident even at $t_d = 8$ µs (Fig. 4). The high-field MFE drastically increases on lowering the temperature (Fig. 2). This indicates that the S-T conversion of the CTE should be caused more effectively by the thermal polarization effect rather than by the Δg effect. In order to observe the magnetic response for the CTE with a small rate constant of S-T conversion, the singlet CTE should have a lifetime longer than the spin conversion time. Figure 5 indicates that the CTE has a lifetime longer than 0.8 s. Therefore, the above-mentioned requirement is fulfilled in this system.

Because the PP is formed after the CTE as shown in Fig. 6, one may be puzzled as to why the MFEs associated with the PP occur earlier than the MFE associated with the CTE. This could be understood by considering that the PP is formed at a time earlier than $t_d = 8$ µs from free polarons generated by the dissociation of the CTE. From the observed delay time dependence of the MFE and energy diagram shown in Fig. 6, the order of the time scale is deduced to be *formation of CTE < formation of PP < T-S conversion of PP < S-T conversion of CTE*.

Summary and conclusion

In this paper, we have reported experiments on the time dependence of MFEs based on photo-CELIV measurements of P3HT:PCBM bulk-heterojunction photovoltaic cells at extremely low temperatures. No MFE associated with the FRE was detected, which is consistent with the large exchange interaction of the FRE. For $t_d \leq 80$ μs, we observed a positive MFE due to the hyperfine-coupling mechanism and a negative MFE due to the Δg mechanism; these MFEs were ascribed to the triplet PP precursor. For $t_d \geq 8$ ms, a positive MFE due to the S-T conversion of the CTE was observed. Based on the photo-CELIV analysis at low temperatures, we estimated the difference in the dissociation energy between the singlet and triplet species of the CTE to be larger than 3 meV. Consequently, the exchange interaction J of the CTE was calculated to be $J > 1.5$ meV. The high-field MFE at low temperature is mainly caused by the thermal polarization effect.

References

1   Z. H. Xiong, D. Wu, Z. V. Vardeny, and J. Shi, *Nature*, 2004, **427**, 821.

2   V. A. Dediu, L. E. Hueso, I. Bergenti, and C. Taliani, *Nat. Mater.*, 2009, **8**, 707.

3   T. D. Nguyen, F. Wang, X.-G. Li, E. Ehrenfreund, and Z. V. Vardeny, *Phys. Rev. B*, 2013, **87**, 075205.

4   K. Ando, S.Watanabe, S.Mooser, E. Saitoh, and H. Sirringhaus, *Nat. Mater.*, 2013, **12**, 622.

5   M. Kimata, D. Nozaki, Y. Niimi, H. Tajima, and Y. Otani, *Phys. Rev. B*, 2015, **91**, 224422.

6   E. L. Frankevich, A. A. Lymarev, I. Sokolik, F. E. Karasz, S. Blumstengel, R. H. Baughman, and H. H. Hörhold, *Phys. Rev. B*, 1992, **46**, 9320.

7   J. Kalinowski, M. Cocchi, D. Virgili, P. Di Marco, and V. Fattori, *Chem. Phys. Lett.*, 2003, **380**, 710.

8   Ö. Mermer, G. Veeraraghavan, T. L. Francis, Y. Sheng, D. T. Nguyen, M. Wohlgenannt, A. Kohler, M. K. Al-Suti, and M. S. Khan, *Phys. Rev. B*, 2005, **72**, 205202.

9   V.N. Prigodin, J.D. Bergeson, D.M. Lincoln, and A. J. Epstein, *Synth. Met.*, 2006, **156** 757.

10   P.A. Bobbert, T. D. Nguyen, F. W. A. van-Oost, B. Koopmans, and M. Wohlgenannt, *Phys. Rev. Lett.*, 2007, **99**, 216801.

11   P. Desai, P. Shakya, T. Kreouzis, W.P. Gillin, N.A. Morley, and M.R.J. Gibbs, *Phys. Rev. B*, 2007, **75**, 094423.

12   B. Hu, L. Yan, and Ming Shao, *Adv. Mater.*, 2009, **21**, 1500.

13   W. Wagemans and B. Koopmans, *Phys. Status Solidi B*, 2011, **248**, 1029.

14   E. Ehrenfreund and Z. V. Vardeny, *Isr. J. Chem.*, 2012, 52, 552.

15   R. N. Mahato, H. Lülf, M. H. Siekman, S. P. Kersten, P. A. Bobbert, M. P. de Jong, L. De Cola, and W. G. van der Wiel1, *Science*, 2013, **341**, 257.

16   R. C. Johnson and R. E. Merrifield, *Phys. Rev. B*, 1970, **1**, 896.

17   Q. Peng, X. Li, and F. Li, *J. Appl. Phys.*, 2012, **112**, 114512.

18   F. Ito, T. Ikoma, K. Akiyama, A. Watanabe, and S. Tero-Kubota, *J. Phys. Chem. B*, 2005, **109**, 8707.

19   G. Juška, K. Genevičius, R. Österbacka, K. Arlauskas, T. Kreouzis, D.D.C. Bradley, and H. Stubb, *Phys. Rev. B*, 2003, **67**, 081201.

20   A.J. Mozer, G. Dennler, N.S. Sariciftci, M. Westerling, A. Pivrikas, R. Österbacka, and G. Juška, *Phys. Rev. B*, 2005, **72**, 035217.

21   M. Pope and C. Swenberg, "Electronic process in Organic Crystals and Polymers"

2nd Ed., Oxford Press, 1999.

22 Y. Kim, S.A. Choulis, J. Nelson, D.D.C. Bradley, S. Cook, and J.R. Durrant, *Appl. Phys. Lett.*, 2005, **86**, 063502.

23 H. Tajima, T. Suzuki, and M. Kimata, *Org. Electron.*, 2012, **13**, 2272.

24 Y. Zhou, C. F.-Hernandez, J. Shim, J. Meyer, A. J. Giordano, H. Li, P. Winget, T. Papadopoulos, H. Cheun, J. Kim, M. Fenoll, A. Dindar, W. Haske, E. Najafabadi, T. M. Khan, H. Sojoudi, S. Barlow, S. Graham, J.-L. Brédas, S. R. Marder, A. Kahn, and B. Kippelen, *Science*, 2012, **336**, 327.

25 G. Juška, K. Arlauskas, M. Viliūnas, and J. Kočka, *Phys. Rev. Lett.*, 2000, **84** 4946.

26 J. Frenkel, *Phys. Rev.*, 1938, **54**, 647.

27 The zero-field studies for the sample used in this measurement have been reported in Ref. 23. The technique applied to evaluate the β value was reported in the same paper.

28 A. Rao, P. C. Y. Chow, S Gélinas, C. W. Schlenker, C.-Z. Li, H.-L. Yip, A. K.-Y. Jen, D. S. Ginger, and R. H. Friend, *Nature*, 2013, **500**, 435.

29 T. M. Clarke and J. R. Durrant, *Chem. Rev.,* 2010**, 110***,* 6736.

30 We added PP state in this diagram in addition to CTE state in order to discuss the MFE observed in this study.

31 H. Hayashi, "Introduction to Dynamic Spin Chemistry; Magnetic Field Effects on Chemichal and Biochemical Reactions", World Scientific Publishing, 2004.

32 J. Wang, A. Chepelianskii, F. Gao, and N. C. Greenham, *Nat. Commun.*, 2012, **3**, 1191.

33 B. Khachatryan, A. H. Devir-Wolfman, L. Tzabari, N. Tessler, Z. V. Vardeny, and E. Ehrenfreund, *Phys. Rev. Appl.*, 2016, **5**, 044001.

34 A. H. Devir-Wolfman, B. Khachatryan, B. R. Gautam, L. Tzabary, A. Keren, N. Tessler, Z. V. Vardeny, and E. Eherenfreund, *Nat. Commun.*, 2014, **5**, 4529.

Table 1 The parameters of the Gaussian functions (Eq. (3)) used to fit the observed density functions of the CTE. The increase of the central energy (ε_0) in the magnetic field of 15 T corresponds to the peak shifts of the CELIV signals.

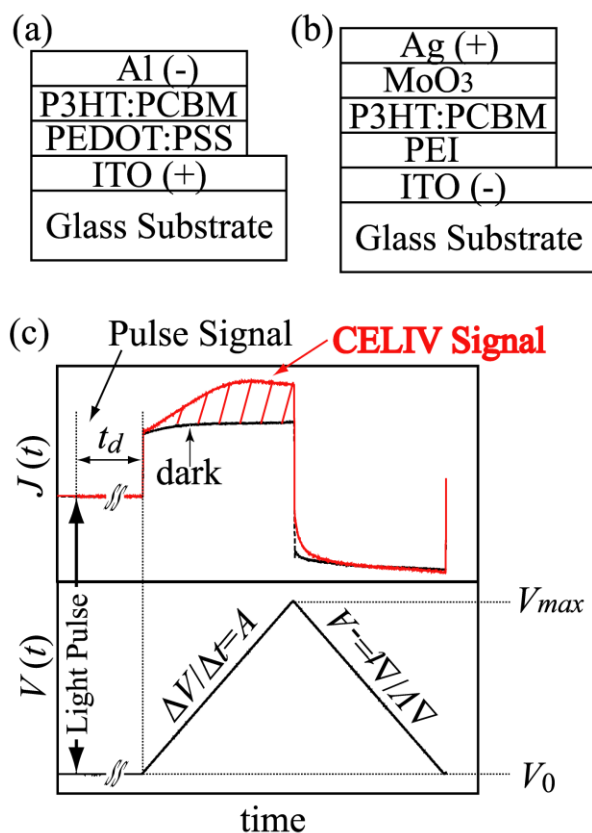|	D (10^{24} states m^{-3} eV^{-1})	ε_0 (eV)	σ(eV)
0 T (1.8 K)	1.0	0.087	0.029
15 T (1.8 K)	1.7	0.094	0.033

Figure Captions

Fig. 1 (a) Conventional polymer bulk-heterojunction photovoltaic cell used for the high-field experiments. The ITO and Al electrodes operate as a cathode and an anode, respectively. The thicknesses of the P3HT:PCBM active layer, PEDOT:PSS hole-transport layer, and Al electrode were 130, 30, and 60 nm, respectively. (b) Inverted-type polymer bulk-heterojunction photovoltaic cell used for the low and intermediate-field experiments. The ITO and Ag electrodes function as an anode and a cathode, respectively. The thicknesses of the PEI, P3HT:PCBM active layer, MoO_3 hole transport layer, and Ag electrode were 10, 100, 15, and 45 nm, respectively. (c) Experimental scheme of photo-CELIV measurements. The symbols $J(t)$ and $V(t)$ on the vertical axis correspond to the extracted current density and reverse-bias voltage, respectively, and t on the horizontal axis denotes the time. V_{max} and V_0 are the maximum and offset applied voltages, correspondingly. In these measurements, photocarriers were generated inside the photovoltaic cell using a light pulse. After a delay time of t_d, carriers were extracted using a linearly ramping reverse-bias voltage with rate A. The offset voltage V_0 was zero except in the pulse signal measurements. To ensure the accuracy of the signal integration, the pulse signal was measured separately under an applied offset voltage of 2.5 V or 3 V.

Fig. 2 (a)-(e) Comparisons of the CELIV signals measured in the magnetic fields $B = 0$ T and 15 T as a function of the electric field. (a) $T = 5$ K, $t_d = 8$ μs, $A = 20000$V/s; (b) $T = 5$ K, $t_d = 800$ ms, $A = 20000$V/s; (c) $T = 1.8$ K, $t_d = 8$ μs, $A = 20000$V/s; (d) $T = 1.8$ K, $t_d = 800$ ms, $A = 20000$V/s; (e) $T = 1.8$ K, $t_d = 8$ ms, $A = 2000$V/s. The green solid lines represent the $B = 0$ T data magnified for comparison.
(f) Density function of the geminate pair, as determined from the CELIV data shown in (e) using Eq. (2). The density functions are well reproduced by the Gaussian functions of Eq. (3) with the parameters of Table 1. The green solid line represents the $B = 0$ T magnified for comparison.

Fig. 3 Measured $MFE(B)$ for $B < 0.2$ T at $T = 2.0$ K. The observed MFE for the pulse signal is rather small. A positive and cusp-like field dependence of $MFE(B)$ is displayed by the CELIV signals for $t_d \leq 3$ ms. For $t_d \geq 8$ ms, $MFE(B)$ is negligible.

Fig. 4 Measured $MFE(B)$ values at $T = 2.0$ K for $B < 3$ T at several t_d. The black solid line shows the least-squares fit of Eq. (4) to the MFE data at $t_d = 8$ μs using the parameters $a = 3.21 \times 10^{-2}$, $B_0 = 0.0112$ (T), and $b = 3.32$ ($T^{-0.5}$). The red line shows the least-squares fit of B^2 to the data at $t_d = 800$ ms. The observed B^2 dependence is consistent with the large value of $MFE(15 \text{ T}) \approx 85\%$ at $t_d = 800$ ms, as shown in Fig. 2.

Fig. 5 Delay time dependence of the CELIV signal intensity at $T = 2.0$ K for the fields $B = 0$, 0.1, and 3 T. Note the logarithmic scale of the horizontal axis. The CELIV signal

exhibits a non-exponential decay as a function of time and an inversion of the MFE at approximately $t_d = 300$ μs. Because the CELIV signal intensity reflects the CTE population, the figure demonstrates that CTE has very long life time at 2.0 K.

Fig. 6   Energy level diagram summarizing the main processes involved in the photocharge generation in the bulk-heterojunction photovoltaic cell. In the photo-CELIV experiments, the charge generation processes (k_{3ST}, k_{6ST}) were controlled through the applied electric field. The S-T (or T-S) conversion and the difference of the reaction rates for the singlet and triplet species induced the MFE on the photocurrent. Because of the exchange interaction, the rate constant of the S-T conversion in the CT exciton is quite small and no S-T conversion is expected in the Frenkel exciton.

Fig. 1 (a) Conventional polymer bulk-heterojunction photovoltaic cell used for the high-field experiments. The ITO and Al electrodes operate as a cathode and an anode, respectively. The thicknesses of the P3HT:PCBM active layer, PEDOT:PSS hole-transport layer, and Al electrode were 130, 30, and 60 nm, respectively. (b) Inverted-type polymer bulk-heterojunction photovoltaic cell used for the low and intermediate-field experiments. The ITO and Ag electrodes function as an anode and a cathode, respectively. The thicknesses of the PEI, P3HT:PCBM active layer, MoO_3 hole transport layer, and Ag electrode were 10, 100, 15, and 45 nm, respectively. (c) Experimental scheme of photo-CELIV measurements. The symbols $J(t)$ and $V(t)$ on the vertical axis correspond to the extracted current density and reverse-bias voltage, respectively, and t on the horizontal axis denotes the time. V_{max} and V_0 are the maximum and offset applied voltages, correspondingly. In these measurements, photocarriers were generated inside the photovoltaic cell using a light pulse. After a delay time of t_d, carriers were extracted using a linearly ramping reverse-bias voltage with rate A. The offset voltage V_0 was zero except in the pulse signal measurements. To ensure the accuracy of the signal integration, the pulse signal was measured separately under an applied offset voltage of 2.5 V or 3 V.
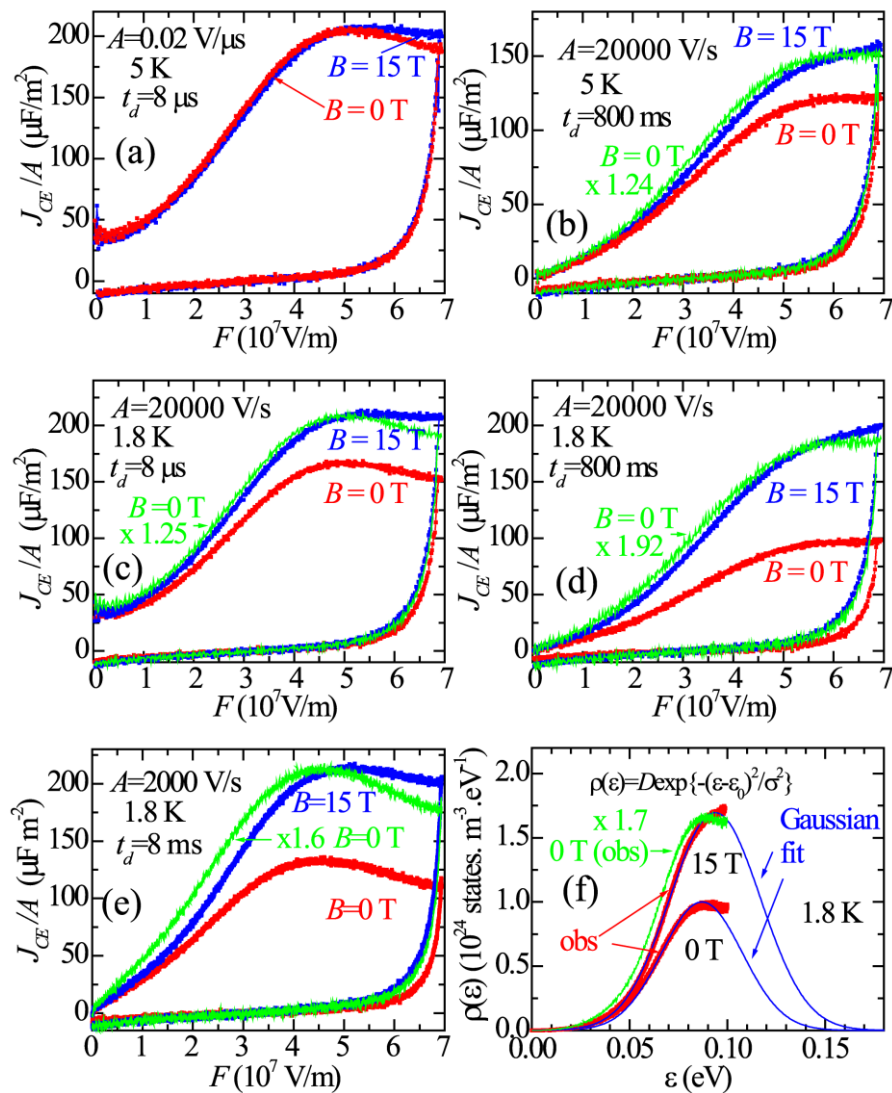
Fig. 2 (a)-(e) Comparisons of the CELIV signals measured in the magnetic fields $B = 0$ T and 15 T as a function of the electric field. (a) $T = 5$ K, $t_d = 8$ μs, $A = 20000$V/s; (b) $T = 5$ K, $t_d = 800$ ms, $A = 20000$V/s; (c) $T = 1.8$ K, $t_d = 8$ μs, $A = 20000$V/s; (d) $T = 1.8$ K, $t_d = 800$ ms, $A = 20000$V/s; (e) $T = 1.8$ K, $t_d = 8$ ms, $A = 2000$V/s. The green solid lines represent the $B = 0$ T data magnified for comparison.

(f) Density function of the geminate pair, as determined from the CELIV data shown in (e) using Eq. (2). The density functions are well reproduced by the Gaussian functions of Eq. (3) with the parameters of Table 1. The green solid line represents the $B = 0$ T magnified for comparison.

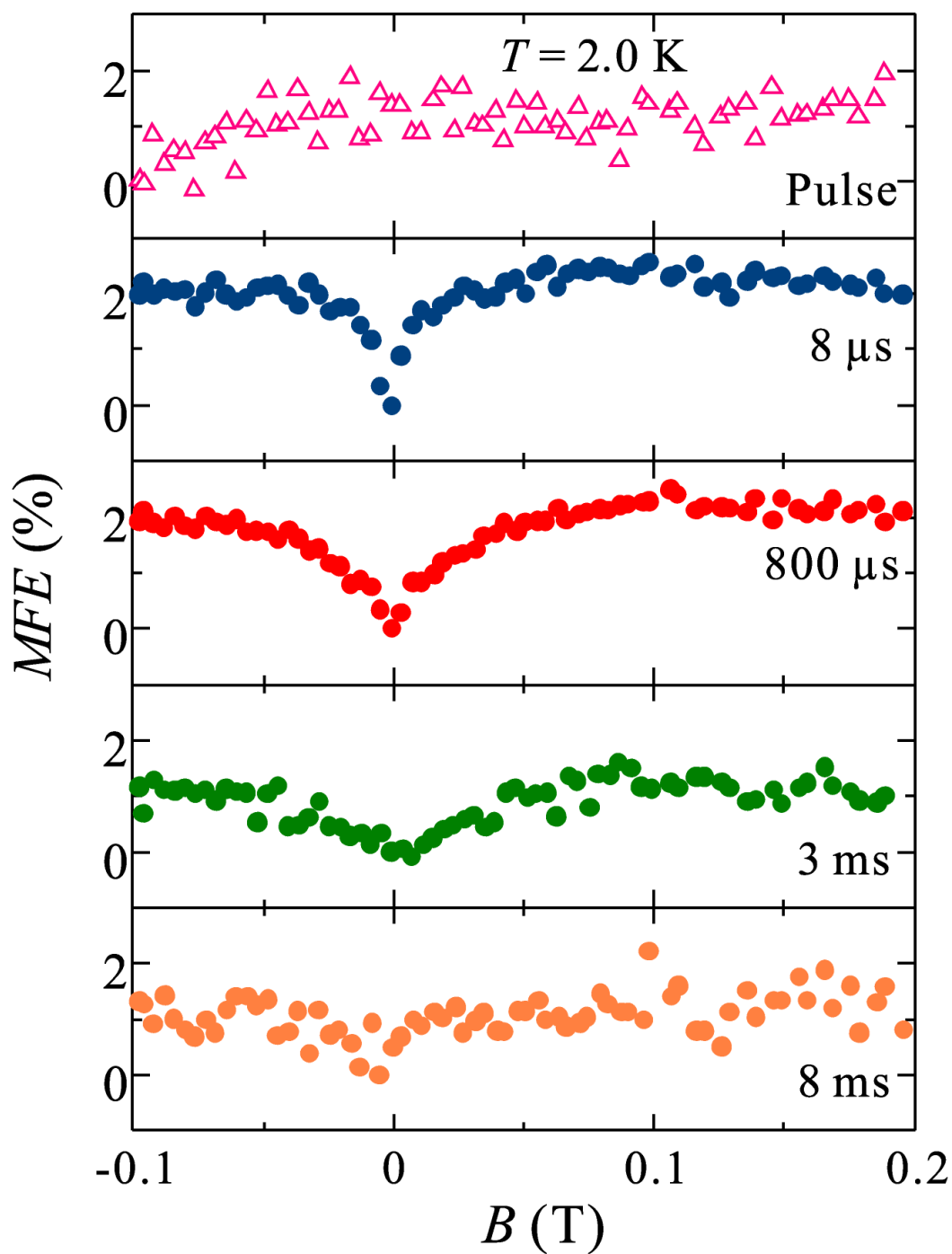Fig. 3 Measured *MFE(B)* for *B* < 0.2 T at *T* = 2.0 K. The observed MFE for the pulse signal is rather small. A positive and cusp-like field dependence of *MFE(B)* is displayed by the CELIV signals for $t_d \leq 3$ ms. For $t_d \geq 8$ ms, *MFE(B)* is negligible.
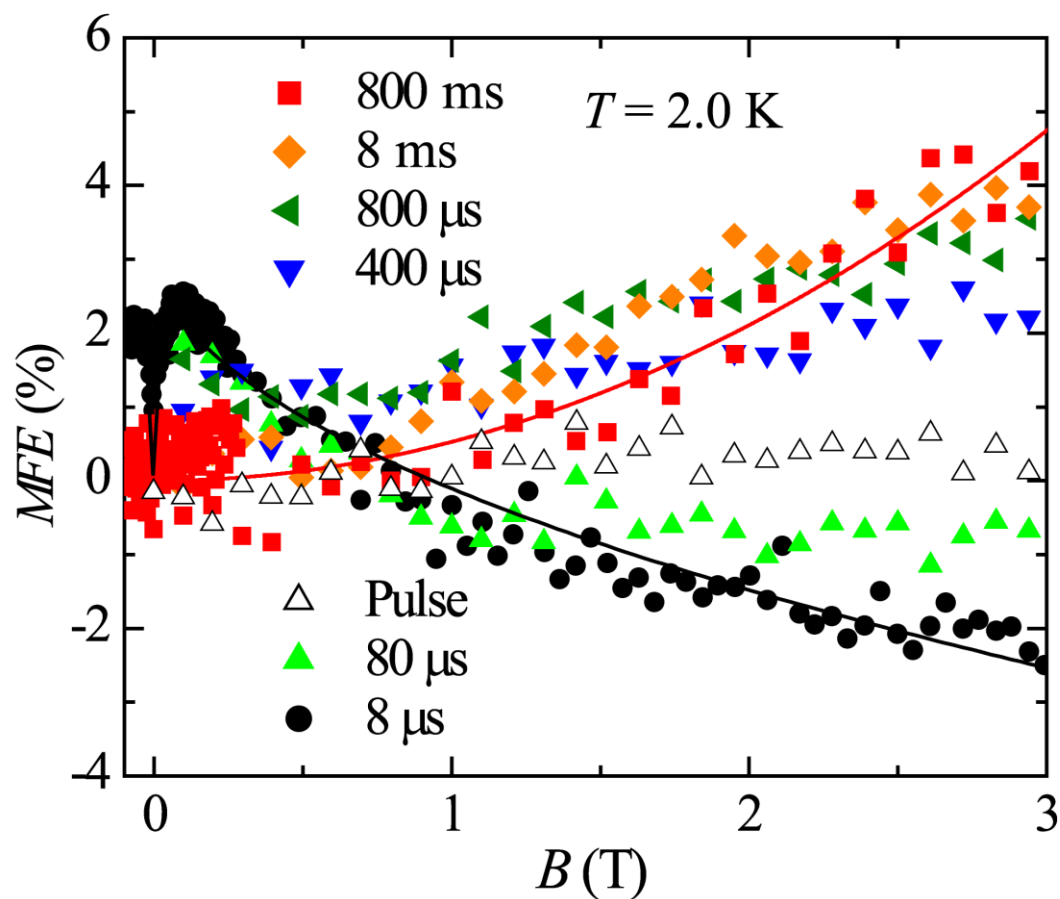
Fig. 4 Measured *MFE*(*B*) values at *T* = 2.0 K for *B* < 3 T at several t_d. The black solid line shows the least-squares fit of Eq. (4) to the MFE data at t_d = 8 μs using the parameters *a* = 3.21×10^{-2}, B_0=0.0112 (T), and *b*=3.32 (T$^{-0.5}$). The red line shows the least-squares fit of B^2 to the data at t_d = 800 ms. The observed B^2 dependence is consistent with the large value of *MFE*(15 T) ≈ 85% at t_d = 800 ms, as shown in Fig. 2.
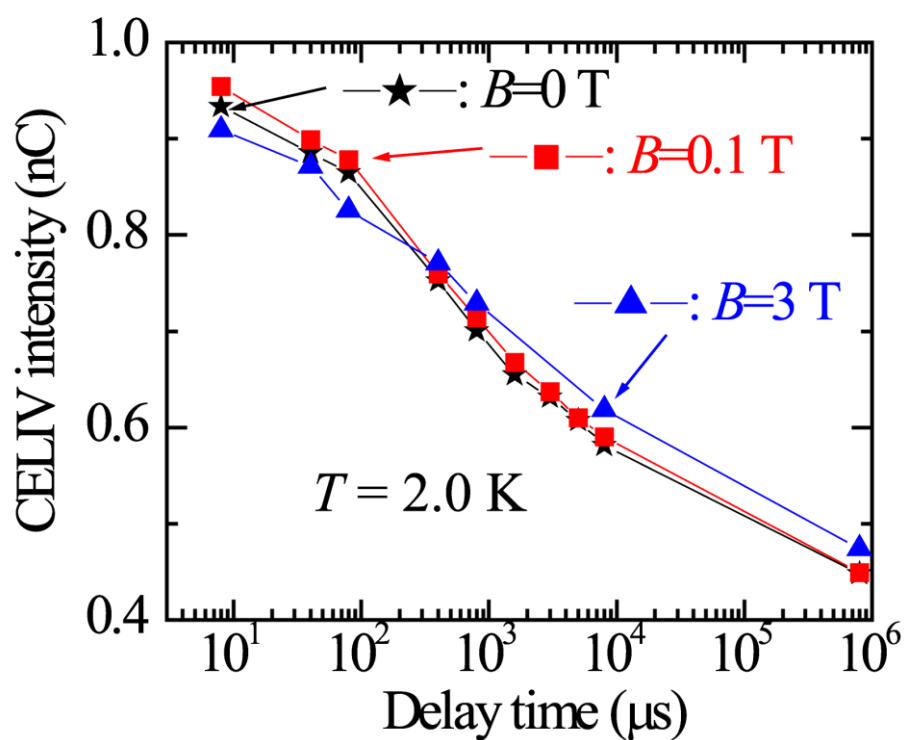
Fig. 5 Delay time dependence of the CELIV signal intensity at $T = 2.0$ K for the fields B = 0, 0.1, and 3 T. Note the logarithmic scale of the horizontal axis. The CELIV signal exhibits a non-exponential decay as a function of time and an inversion of the MFE at approximately t_d = 300 μs. Because the CELIV signal intensity reflects the CTE population, the figure demonstrates that CTE has very long life time at 2.0 K.
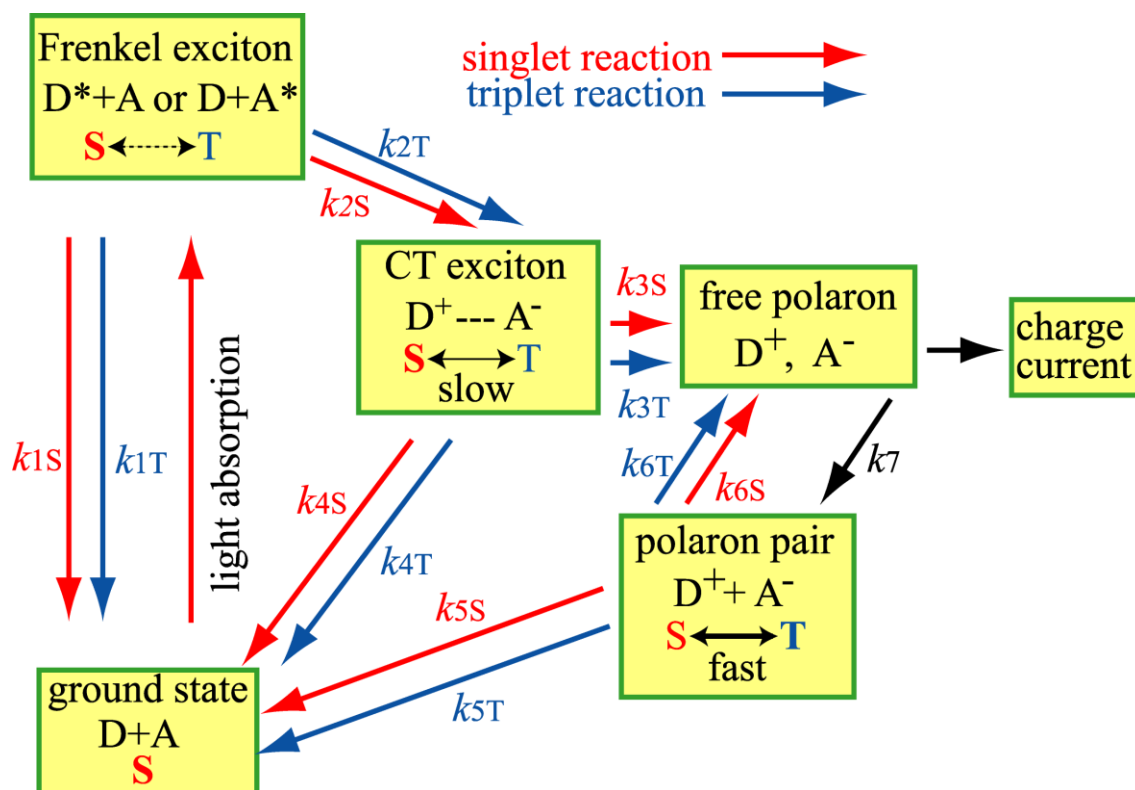
Fig. 6   Energy level diagram summarizing the main processes involved in the photocharge generation in the bulk-heterojunction photovoltaic cell. In the photo-CELIV experiments, the charge generation processes (k_{3ST}, k_{6ST}) were controlled through the applied electric field. The S-T (or T-S) conversion and the difference of the reaction rates for the singlet and triplet species induced the MFE on the photocurrent. Because of the exchange interaction, the rate constant of the S-T conversion in the CT exciton is quite small and no S-T conversion is expected in the Frenkel exciton.